Superconducting phase transitions in thin mesoscopic rings with enhanced surface superconductivity

Guo-Qiao Zha,* Shi-Ping Zhou,† Bao-He Zhu, Yao-Ming Shi, and Hong-Wei Zhao
Department of Physics, Shanghai University, 99 Shangda Road, Shanghai 200444, People's Republic of China
(Received 18 April 2006; revised manuscript received 15 May 2006; published 28 July 2006)

The superconducting phase transitions between different vortex states with the magnetic field for a thin mesoscopic superconducting ring surrounded by a medium that enhanced its superconductivity near the boundary are investigated by the phenomenological Ginzburg-Landau theory. The transitions between different giant vortex states and between the giant vortex and multivortex states with $\Delta L>1$ (L is the vorticity of the vortex state) are found for a small ring with increasing surface enhancement. The influences of the surface enhancing superconducting effect and the inner radius as well as the temperature on phase transition are studied by examining the H-$|\xi/b|$, H-R_i, and H-T phase diagrams, respectively. Further increasing the effect of enhanced surface superconductivity, we find the reentrant transition with the same vorticity and the transitions between the stable multivortex states with $\Delta L>1$ for different ring inner radii. We also investigate the vortex configurations for a relatively large ring, and the vortex state with two stable vortex shells can be found as the ground state due to the enhanced surface superconductivity.

DOI: 10.1103/PhysRevB.74.024527 PACS number(s): 74.20.De, 74.25.Op, 74.25.Dw

I. INTRODUCTION

A mesoscopic sample is such that its size is comparable to the magnetic-field penetration depth λ or the coherence length ξ. Previously, the samples of different shapes surrounded by vacuum or an insulator medium have been considered extensively both experimentally[1] and theoretically.[2–8] It has been shown that two kinds of superconducting state can exist in these samples, i.e., the giant vortex state and the multivortex state. The giant vortex state has cylindrical symmetry and is stable in small size due to the confinement effect. Meanwhile, the giant vortex state can break up into multivortices for sufficiently large size and the transition between such states is described by the saddle-point state, which corresponds to the energy barrier state between those states. For the vortex phase transitions in mesoscopic superconducting disks, the vorticity L always changes with one unit at the penetration field,[3] and several vortices can simultaneously enter into the system for sufficiently large radius.[4] Palacios calculated the saddle points or energy barriers that prevent the vortex escape and entrance in superconducting mesoscopic disks[5] as well as the vortex configurations with two stable vortex shells (or rings) in disks with larger radius[6] using the lowest Landau level approximation. The transitions between the different vortex states of thin mesoscopic superconducting disks and rings have been studied by Baelus *et al.*,[7] and the $L\leftrightarrow L+1$ transition between two giant vortex states in small system as well as the transitions between a multivortex state and a giant vortex state and between two multivortex states in larger sizes were obtained. For the transitions between different vortex states in superconducting disks with a sufficiently large radius such that several shells of vortices can be stabilized, the change in vorticity can be larger than one with increasing and decreasing magnetic field comparing with small disks.[8]

Apart from the size and geometry, the vortex properties of a mesoscopic superconductor are strongly influenced by the boundary condition. For a superconductor in contact with a medium with surface enhancement or suppression of superconductivity, we have the general boundary condition[9,10]

$$\vec{n}\cdot(-i\vec{\nabla}-\vec{A})\psi|_s=\frac{i}{b}\psi|_s, \tag{1}$$

where $\vec{n}$ is the unit vector normal to the sample surface, $\vec{A}$ is the vector potential, ψ is the order parameter, and b is the surface extrapolation length, which is the effective penetration depth of the order parameter into the surrounding medium. For both the superconductor-vacuum and the superconductor-insulator boundary, one has $b\rightarrow\infty$. The case $b>0$ corresponds to surface suppression of the superconducting order parameter and this case has been studied in Ref. 11 for mesoscopic cylinders. The opposite case $b<0$ corresponds to surface enhancement of superconductivity. The vortex properties of mesoscopic thin disks and infinitely long cylinders as well as thin rings with enhanced surface superconductivity were studied in Refs. 12–14, respectively. It has been found that increasing the superconductivity near the surface leads to higher critical fields and critical temperatures, and the multivortex state can be stabilized by the surface enhancement of superconductivity and can be found as the ground state. Moveover, the phase transitions between states with $\Delta L>1$ can be found in small disks with enhanced surface superconductivity for a small maximum value of vorticity or at magnetic fields close to the superconducting/normal transition point.[12]

In the present paper, we investigate the phase transitions between different vortex states with increasing or decreasing the magnetic field for thin mesoscopic superconducting rings surrounded by a medium which enhances superconductivity at the sample surface through the phenomenological Ginzburg-Landau theory. The ring has more than one boundary in comparison with the disk sample, and the disk is a special case of the ring with zero inner radius. We generalize the method in Ref. 15 and present a systematic study of the phase transition for the mesoscopic rings with a fixed thick-

ness. We find the transitions between different giant vortex states and between the giant vortex and multivortex states with $\Delta L>1$, which can only exist in large size when the parameter $1/b$ tends to zero, for a small ring with increasing surface enhancement. For the influences of the surface enhancement and the inner radius as well as the temperature on phase transition, we give the H-$|\xi/b|$, H-R_i, and H-T phase diagrams, respectively. Further increasing the surface enhancement, we find the reentrant transition ("*giant vortex* $\rightarrow$ *multivortex* $\rightarrow$ *giant vortex*") with the same vorticity and the transitions between the stable multivortex states with $\Delta L>1$ for different ring inner radii. The vortex configurations for a relatively large ring are also investigated finally and we find that the vortex state with two stable vortex shells can exist in the ground state due to the enhanced surface superconductivity.

The paper is organized as follows. In Sec. II, we present our theoretical model and give the necessary formalism. The different kinds of phase transitions as well as the H-$|\xi/b|$, H-R_i, and H-T phase diagrams for the small rings are presented in Sec. III. In Sec. IV, the vortex configurations and transitions between different stable states for the larger rings are studied. Our results are summarized in Sec. V.

II. THEORETICAL APPROACH

We consider mesoscopic superconducting rings with outer radius R_o and inner radius R_i and thickness d. We restrict ourselves to sufficiently thin rings such that $d \ll \xi, \lambda$. In this case, the external magnetic field $\vec{H}$ is uniform and directed normal to the rings plane. The Cooper pair density $|\psi(\vec{r})|^2$ is determined from a solution of coupled nonlinear GL equations for the superconducting order parameter $\psi(\vec{r})$ and the magnetic field $\vec{h}(\vec{r})=\vec{\nabla}\times\vec{A}(\vec{r})$

$$(-i\vec{\nabla}-\vec{A})^2\psi=\psi-\psi|\psi|^2, \tag{2}$$

$$\kappa^2\vec{\nabla}\times\vec{\nabla}\times\vec{A}=\vec{j}, \tag{3}$$

where the density of the superconducting current $\vec{j}$ given by

$$\vec{j}=\frac{1}{2i}(\psi^*\vec{\nabla}\psi-\psi\vec{\nabla}\psi^*)-|\psi|^2\vec{A}. \tag{4}$$

We use the cylindrical coordinates $\vec{r}=(\rho,\theta,z)$ and choose the gauge $\vec{A}=(H\rho/2)\vec{e}_\theta$, where ρ is the radial distance from the cylinder axis z, and θ is the azimuthal angle. The ring lies between $z=d/2$ and $-d/2$. We measure the distance in units of the coherence length ξ and the magnetic field in $H_{c2}=c\hbar/2e\xi^2=\kappa\sqrt{2}H_c$, and the superconducting current in $j_0=cH_c/2\pi\xi$, where H_c is the thermodynamic critical field and $\kappa=\lambda/\xi$ is the GL parameter. The free energy of the superconducting state, measured in $F_0=H_c^2V/8\pi$ units, is expressed as

$$F=\frac{2}{V}\left[\int dV\left(-|\psi|^2+\frac{1}{2}|\psi|^4+|-i\vec{\nabla}\psi-\vec{A}\psi|^2+\kappa^2[\vec{h}(\vec{r})-\vec{H}]^2\right)+\frac{1}{b}\oint dS|\psi|^2\right]. \tag{5}$$

The last term in Eq. (5) is the surface contribution, which reduces the free energy when $b<0$, implying the superconductivity enhanced effect.

For the multivortex state, the order parameter can expressed as a superposition of giant vortex states with different L_j,

$$\psi(\vec{\rho})=\sum_{L_j=0}^{L}C_{L_j}f_{L_j}(\rho)\exp(iL_j\theta), \tag{6}$$

where L is equal to the number of vortices in the ring or it is the effective total angular momentum of a vortex state. For the transitions between a multivortex state and a giant vortex state and between different multivortex states, we consider states that are built up by three components in Eq. (6),

$$\psi(\vec{\rho})=C_{L_1}f_{L_1}(\rho)\exp(iL_1\theta)+C_{L_2}f_{L_2}(\rho)\exp(iL_2\theta)+C_{L_3}f_{L_3}(\rho)\exp(iL_3\theta), \tag{7}$$

where $L_1<L_2<L_3$. Then the energy of the multivortex state becomes

$$F_{L_1,L_2,L_3}=C_{L_1}^4A_{L_1}+C_{L_2}^4A_{L_2}+C_{L_3}^4A_{L_3}+4C_{L_1}^2C_{L_2}^2A_{L_1,L_2}+4C_{L_2}^2C_{L_3}^2A_{L_2,L_3}+4C_{L_1}^2C_{L_3}^2A_{L_1,L_3}+2\Lambda_{L_1}C_{L_1}^2B_{L_1}+2\Lambda_{L_2}C_{L_2}^2B_{L_2}+2\Lambda_{L_3}C_{L_3}^2B_{L_3}, \tag{8}$$

where

$$A_{L_j}=\frac{2\pi d}{V}\int_{R_i}^{R_o}\rho d\rho f_{L_j}^4(\rho), \tag{9}$$

$$A_{L_j,L_k}=\frac{2\pi d}{V}\int_{R_i}^{R_o}\rho d\rho f_{L_j}^2(\rho)f_{L_k}^2(\rho), \tag{10}$$

$$B_{L_j}=\frac{2\pi d}{V}\int_{R_i}^{R_o}\rho d\rho f_{L_j}^2(\rho), \tag{11}$$

and $f_{L_j}(\rho)$ as well as Λ_{L_j} have been shown in Ref. 15. The trial function $f_{L_j}(\rho)$ can be expressed as a linear combination of two confluent hypergeometric functions (or first and second types of Kummer functions) M and U.[16]

For the three-component approximation, the accuracy has been discussed in Ref. 17, and the authors considered a state described by a three-component approximation and by a five-component one. They showed that the energies found for a different number of components differ by less than 0.2%, suggesting that the three-component approach is applicable. Also, it would unlikely bring serious problems in determining the transition field value, and the uncertainty is then estimated to be less than 4.5% since the magnetic-field square is proportional to the density of energy. Moreover, for the three-component solutions (two vortex shells), the energy

functional is invariant for all the three phases whenever $L_1+L_3\neq 2L_2$.[6] Although the relative angular positions of vortices depend on the phases when $L_1+L_3=2L_2$, there is an obvious choice for these phases: $\phi_{L_1}=0$, $\phi_{L_2}=0$, and $\phi_{L_3}=\pi$, which gives a negative contribution to the free energy that reflects a lock-in position between the vortex shells.[6] So the coefficient C_{L_j}, which should be a complex number in general, can be treated as a real number for our three-component state, in particular when $L_1+L_3\neq 2L_2$. Through minimization of Eq. (8) with respect to C_{L_1}, C_{L_2}, and C_{L_3}, we can determine the parameters $\{C_{L_j}\}$,

$$C_{L_1} = \pm[(2\Lambda_{L_2}A_{L_3}B_{L_2}A_{L_1,L_2}+2\Lambda_{L_3}A_{L_2}B_{L_3}A_{L_1,L_3} + 4\Lambda_{L_1}B_{L_1}A_{L_2,L_3}^2-\Lambda_{L_1}A_{L_3}B_{L_1}A_{L_2}-4\Lambda_{L_2}A_{L_1,L_3}A_{L_2,L_3}B_{L_2} - 4\Lambda_{L_3}A_{L_1,L_2}A_{L_2,L_3}B_{L_3})/(16A_{L_1,L_2}A_{L_1,L_3}A_{L_2,L_3} - 4A_{L_2,L_3}^2A_{L_1}-4A_{L_1,L_2}^2A_{L_3}-4A_{L_1,L_3}^2A_{L_2}+A_{L_1}A_{L_2}A_{L_3})]^{1/2}, \quad (12)$$

$$C_{L_2} = \pm[(2\Lambda_{L_1}A_{L_3}B_{L_1}A_{L_1,L_2}+2\Lambda_{L_3}A_{L_1}B_{L_3}A_{L_2,L_3} + 4\Lambda_{L_2}B_{L_2}A_{L_1,L_3}^2-\Lambda_{L_2}A_{L_3}B_{L_2}A_{L_1}-4\Lambda_{L_3}A_{L_1,L_2}A_{L_1,L_3}B_{L_3} - 4\Lambda_{L_1}A_{L_1,L_3}A_{L_2,L_3}B_{L_1})/(16A_{L_1,L_2}A_{L_1,L_3}A_{L_2,L_3} - 4A_{L_2,L_3}^2A_{L_1}-4A_{L_1,L_2}^2A_{L_3}-4A_{L_1,L_3}^2A_{L_2}+A_{L_1}A_{L_2}A_{L_3})]^{1/2}, \quad (13)$$

$$C_{L_3} = \pm[(2\Lambda_{L_2}A_{L_1}B_{L_2}A_{L_2,L_3}+2\Lambda_{L_1}A_{L_2}B_{L_1}A_{L_1,L_3} + 4\Lambda_{L_3}B_{L_3}A_{L_1,L_2}^2-\Lambda_{L_3}A_{L_1}B_{L_3}A_{L_2}-4\Lambda_{L_2}A_{L_1,L_2}A_{L_1,L_3}B_{L_2} - 4\Lambda_{L_1}A_{L_2,L_3}A_{L_1,L_2}B_{L_1})/(16A_{L_1,L_2}A_{L_1,L_3}A_{L_2,L_3} - 4A_{L_2,L_3}^2A_{L_1}-4A_{L_1,L_2}^2A_{L_3}-4A_{L_1,L_3}^2A_{L_2}+A_{L_1}A_{L_2}A_{L_3})]^{1/2}. \quad (14)$$

Note: In our derivation, the weak correlation term between vortices when $L_1+L_3=2L_2$, i.e.,

$$4\delta_{L_1+L_3,2L_2}C_{L_1}C_{L_3}C_{L_2}^2 * \left(\frac{2\pi d}{V}\int_{R_i}^{R_o}\rho d\rho f_{L_1}(\rho)f_{L_3}(\rho)f_{L_2}^2(\rho)\right), \quad (15)$$

had been omitted in Eq. (8). This approximation is justified. We checked the free energies of the vortex state with and without the correlation term and found that the contribution of the correlation term is very small (the relative deviation is less than 0.1%).

For nonzero temperature T, the temperature dependence of ξ, H_{c2} is assumed as

$$\xi(T)=\frac{\xi(0)}{\sqrt{|1-T/T_{c0}|}}, \quad H_{c2}(T)=H_{c2}(0)|1-T/T_{c0}|, \quad (16)$$

where T_{c0} is the critical temperature at zero magnetic field for the normal boundary condition, i.e., $|\xi(0)/b|=0$. We will only use $\xi(0)$ and $H_{c2}(0)$ as the basis for our units when we consider the H-T phase diagrams.

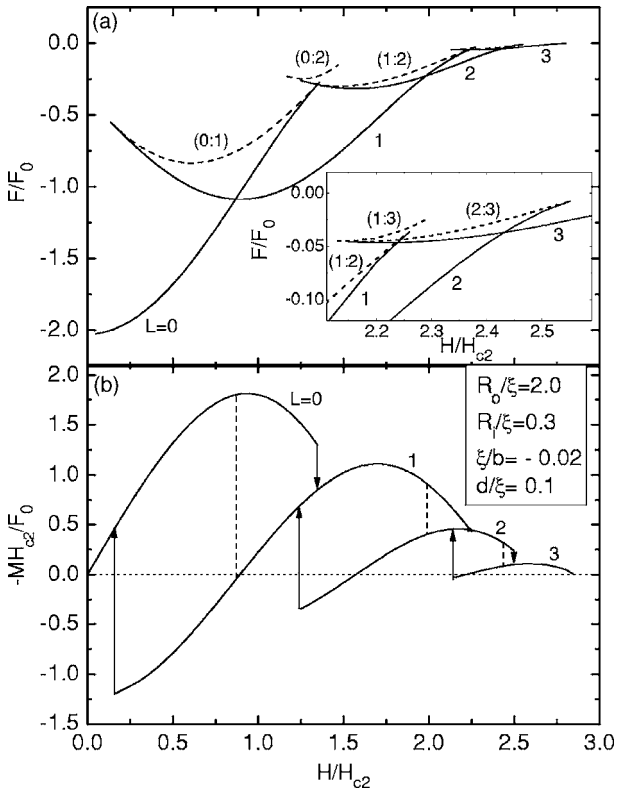

FIG. 1. (a) Free energy and (b) magnetization of the ground state and the saddle-point states in a superconducting ring with $R_o=2.0\xi$ and $R_i=0.3\xi$ and $\xi/b=-0.02$. The different giant vortex and saddle-point states are shown by the solid and dashed curves, respectively. The vertical dashed lines give the ground-state transitions.

III. SMALL RINGS

First, we investigate the phase transitions between states with different vorticity L under the effect of enhanced surface superconductivity for small superconducting rings with fixed outer radius $R_o=2.0\xi$ and thickness $d=0.1\xi$. Figure 1 shows the free energies F and the corresponding magnetization $M=-\partial F/\partial H$ curves of the equilibrium vortex states for a ring with $R_i=0.3\xi$ and $\xi/b=-0.02$. The giant vortex states (solid curves) are denoted as their L values and the saddle-point states (dashed curves) as $(L_1:L_2)$, which set a barrier for state transition between L_1 and L_2. The L_1 and L_2 states correspond to the minima of the free energy in functional space, and the lowest barrier between those two minima is a saddle point. The vertical dashed lines in Fig. 1(b) show the transition fields $H_{\rm tr}$, where the ground-state transitions from L to $L+1$ would occur for a sample of body. Due to an energy barrier between the states with vortivity L_1 and L_2, the L_1 state can remain stable up to the penetration field $H_p(>H_{\rm tr})$ and transits to the L_2 state with increasing applied field, and for decreasing field the L_2 state can remain stable down to the expulsion field $H_e(<H_{\rm tr})$ and the transition between the L_1 and L_2 states can occur. In Fig. 1(a), there do not exist stable multivortex states for $\xi/b=-0.02$ and the phase transitions $0\rightarrow 1\rightarrow 2\rightarrow 3\rightarrow$ "*Normal state*" can occur with increasing field, and "*Normal state*" $\rightarrow 3\rightarrow 2\rightarrow 1\rightarrow 0$

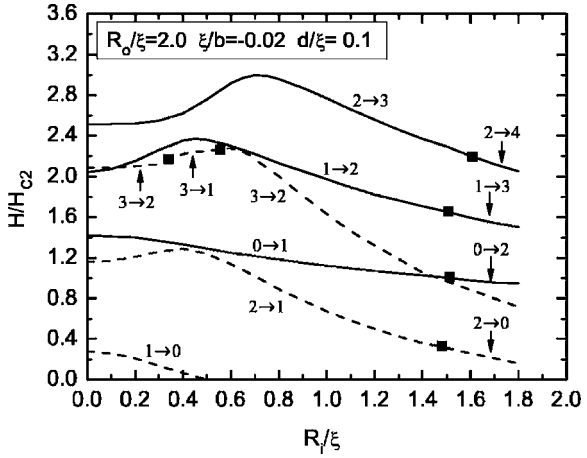

FIG. 2. The penetration field H_p (solid curves) and the expulsion field H_e (dashed curves) as a function of the inner radius R_i for a ring with $R_o=2.0\xi$ and $\xi/b=-0.02$ for $L\leqslant 3$. The solid squares denote the critical inner radii where the number of penetrating/expulsing vortices changes.

with decreasing field. These transitions are given in Fig. 1(b) by the arrows. For the influence of the inner radius on phase transition, we plot the penetration fields H_p (solid curves) and the expulsion fields H_e (dashed curves) as a function of the inner radius R_i for the rings with $\xi/b=-0.02$ and fixed outer radius $R_0=2.0\xi$ for $L\leqslant 3$ in Fig. 2. The solid squares denote the critical inner radii where the number of vortices changes. We see that the H_e for the $L=1$ state and the H_p for the $L=0$ state decrease with increasing the inner radius, and for the other states the H_e and H_p increase first to maxima and then decrease. Moreover, for very large inner radii the transitions with $\Delta L=2$ can occur in general. Surprisingly, with decreasing field, the $3\rightarrow 1$ transition occurs when the inner radius varies in the range of $0.32\xi\leqslant R_i\leqslant 0.51\xi$ and for the larger inner radii we only find the $3\rightarrow 2$ transition. Figure

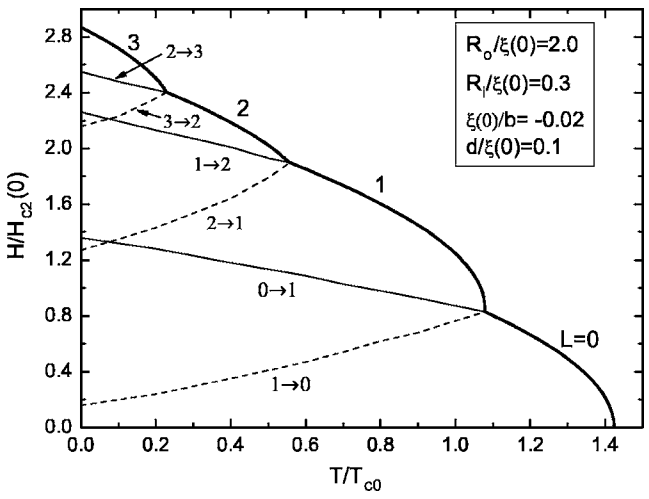

FIG. 3. The H-T phase diagram for a ring with $R_o=2.0\xi(0)$ and $R_i=0.3\xi(0)$ and $\xi(0)/b=-0.02$. The thick curve indicates the superconducting/normal transition. The thin solid curves are the boundaries of the stability regions for increasing magnetic field and the thin dashed curves are the boundaries for decreasing field.

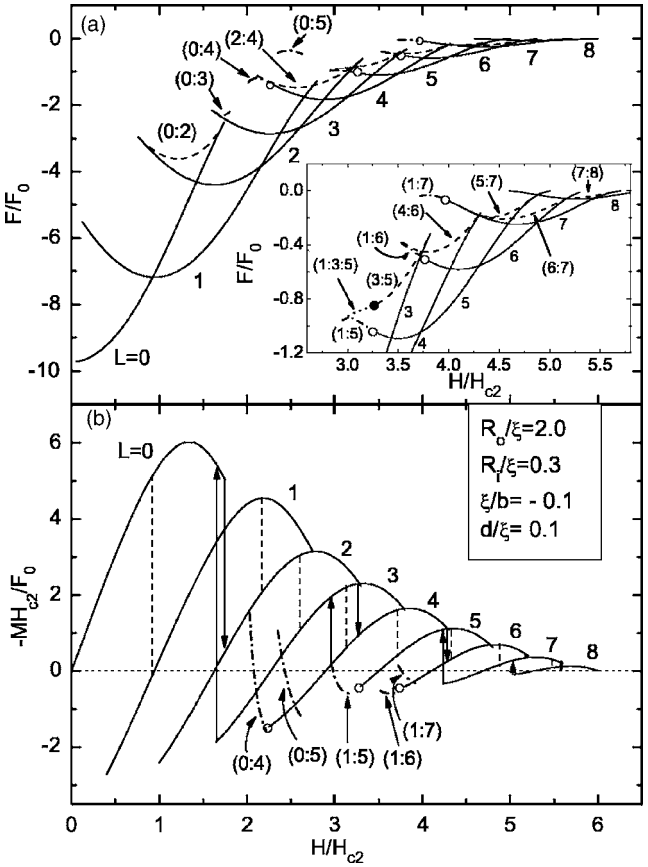

FIG. 4. The same as Fig. 1 but for $\xi/b=-0.1$. The metastable states are shown by the dash-dotted curves. The open circles indicate the multivortex to giant vortex transition fields. The solid circle in the inset denotes the transition field from the (1:5) stable state to the (3:5) state.

3 gives the H-T phase diagram for a superconducting ring with $R_o=2.0\xi(0)$, $R_i=0.3\xi(0)$, and $\xi(0)/b=-0.02$. The thick solid curve indicates the superconducting/normal transition with the corners showing the switching between different L states. The thin solid curves are the boundaries for a preceding stable state with increasing magnetic field and the thin dashed curves are the boundaries with decreasing field. Therefore, together with the superconducting/normal transition boundary, they define the regime where the state L is stable in the phase space.

It has been shown that, because of the enhanced surface superconductivity, the multivortex states can become stable with increasing values of $|\xi/b|$ in small rings.[14] Figure 4(a) shows the free energies and Fig. 4(b) the corresponding magnetization curves of the equilibrium vortex states for a ring with $R_i=0.3\xi$ and $\xi/b=-0.1$. The multivortex states (dash-dotted curves) are denoted as $(L_1:L_2)$, where L_1 and L_2 are the angular momentum values of which the multivortex states are composed. From Fig. 4(a), we can find that the multivortices can exist as the metastable states, meanwhile the phase transitions become more complicated. Just like the disk sample,[12] we find that the transitions with $\Delta L>1$ can occur [see the arrows in Fig. 4(b)]: $0\rightarrow 2\rightarrow 4\rightarrow 6\rightarrow 7\rightarrow 8\rightarrow$ "*Normal state*" with increasing field and "*Normal state*" $\rightarrow 8\rightarrow 7\rightarrow 5\rightarrow (1:5)\rightarrow 3\rightarrow 0$ with decreas-

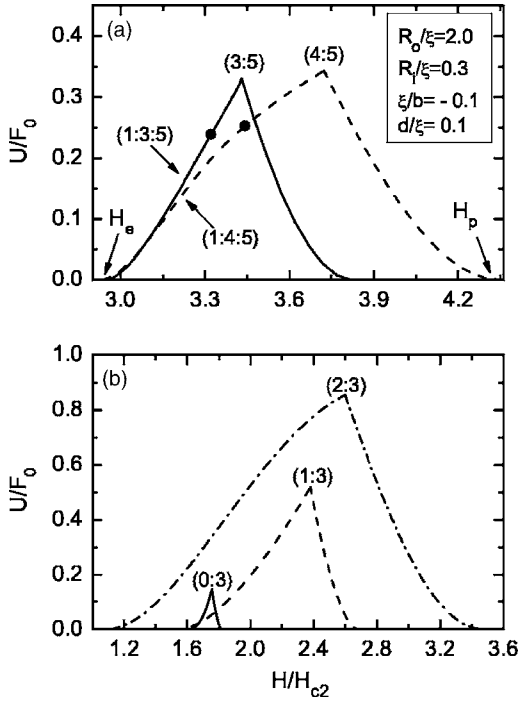

FIG. 5. The energy barriers U corresponding to the transitions $(1:5)\rightarrow 3$ (a) and $3\rightarrow 0$ (b) (solid curves) and the other possible transitions (dashed and dash-dotted curves). The solid circles in (a) denote the transition fields from the (1:5) stable state to the (3:5) or (4:5) unstable states.

ing field. The transition between the (1:5) metastable state and the $L=3$ giant vortex state with decreasing field is realized through the intermediate saddle-point state (1:3:5), i.e., the (1:5) state transits to the (3:5) saddle-point state first and then to the $L=3$ state.

As an example, Fig. 5 gives the energy barriers U corresponding to the transitions $(1:5)\rightarrow 3$ (a) and $3\rightarrow 0$ (b) (solid curves), and those for $(1:5)\rightarrow 4$ as well as $3\rightarrow 2$ and $3\rightarrow 1$ are indicated by the dashed and dash-dotted curves. The transition fields from the (1:5) stable state to the (3:5) and (4:5) states are given by the solid circles in Fig. 5(a). We can see that the barriers between the (1:5) and $L=3$ states as well as between the $L=3$ and $L=0$ states have the lowest values and the expulsion fields H_e have the largest values. Figures 6(a)–6(c) and 6(e)–6(g) show the contour plots of the Cooper-pair density for the (1:3:5) and (3:5) saddle-point states at different magnetic fields, respectively. Figures 6(d) and 6(h) show the phase contour plots corresponding to Figs. 6(c) and 6(g), respectively. Phases near the zero are given by white regions and near 2π by dark regions. We can find that one vortex is in the hole while the other four vortices are located on one shell for the metastable (1:5) state. With increasing field, two vortices near the outer boundary move towards, the center and the other two vortices near the outer boundary move into the ring for the (1:3:5) state. We can see the positions of the vortices clearly from Fig. 6(d) at $H/H_{c2}=3.32$ when the (1:3:5) state transits to the (3:5) saddle-point state. After transiting to (3:5) state, two vortices will move outside of the system with increasing field and then form the $L=3$ giant vortex state. In Fig. 6(h), the phase

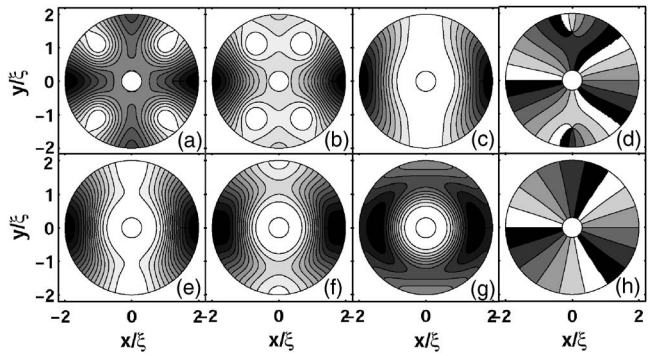

FIG. 6. Contour plot of the Cooper-pair density and phase of the order parameter (d) and (h) for a ring with $R_o=2.0\xi$ and $R_i=0.3\xi$ and $\xi/b=-0.1$ corresponding to the (1:3:5) saddle-point state (a), (b), and (c) as well as the (3:5) state (e), (f), and (g) at $H/H_{c2}=2.95$, 3.1, 3.32, 3.5, 3.7, and 3.82, respectively. Light and dark regions correspond to low and high Copper-pair density. Phases near zero are given by white regions and near 2π by dark regions.

difference $\Delta\varphi=3\times 2\pi$ when encircling the superconductor near the outer boundary, which means vorticity $L=3$. For the (0:3) saddle-point state, Fig. 7 shows the contour plots of the Cooper-pair density and phase of the order parameter at different magnetic fields. With increasing field, three vortices move from the center to the outer region of the ring, and the state changes from $L=3$ to $L=0$, as shown in Figs. 7(a)–7(d) for the Cooper-pair density and in Figs. 7(e)–7(h) of the phase of the order parameter.

With increasing the ring inner radius, the phase transitions will become more complicated. As an example, the phase transitions and the expulsion fields H_e for vorticity $L=5$ and 6 for the rings with $R_o=2.0\xi$ and $\xi/b=-0.1$ and different inner radii R_i are given in Table I. With increasing the inner radius, the (1:5) and (2:6) states can be found as the metastable states, whereas the (0:5) and (1:6) metastable states disappear.[14] So we can find the transitions from different multivortex states to the giant vortex states with increasing inner radius. However, for the large inner radii only the transitions between different giant vortex states can exist.

In Fig. 8, we plot the H-T phase diagram for a ring with $R_o=2.0\xi(0)$, $R_i=0.3\xi(0)$, and $\xi(0)/b=-0.1$. The solid

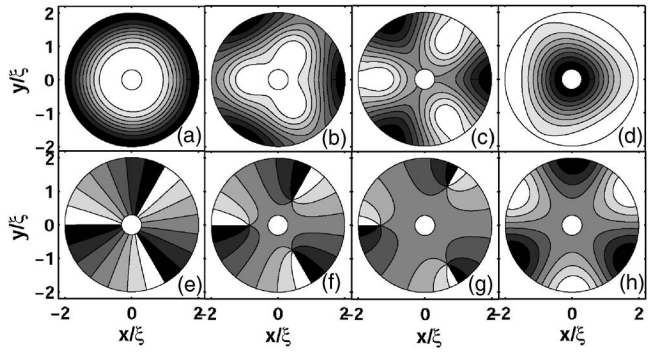

FIG. 7. Contour plot of the Cooper-pair density and phase of the order parameter for a ring with $R_o=2.0\xi$ and $R_i=0.3\xi$ and $\xi/b=-0.1$ corresponding to the (0:3) saddle-point state at $H/H_{c2}=1.604$, 1.64, 1.75, and 1.819, respectively.

TABLE I. The phase transitions as well as the expulsion fields $H_{e,5}$ and $H_{e,6}$ for $L=5$ and 6 for rings with $\xi/b=-0.1$ and fixed outer radius $R_o=2.0\xi$ and different inner radii R_i.

R_i/ξ	$L=5$	$H_{e,5}/H_{c2}$	$L=6$	$H_{e,6}/H_{c2}$
0	(0:5)→3	2.802	6→4	3.52
0.1	(0:5)→3	2.801	6→4	3.52
0.15	5→1	2.857		
0.2	(1:5)→3	2.907	6→4	3.521
0.3	(1:5)→3	2.944	(1:6)→4	3.532
0.4	(1:5)→4	2.954	(1:6)→4	3.539
0.5	(1:5)→3	2.963	(1:6)→4	3.545
0.6	5→2	3.27	(2:6)→5	3.738
0.7	5→2	3.55	(2:6)→5	3.768
0.74			(2:6)→4	3.77
0.8	5→2	3.22	6→3	4.01
0.9	5→3	3.03	6→3	3.92
1	5→3	2.84	6→4	3.72
1.1	5→3	2.61	6→4	3.47
1.2	5→3	2.38	6→4	3.2
1.3	5→3	2.17	6→4	2.93
1.4	5→3	1.98	6→4	2.69
1.5	5→3	1.8	6→4	2.46
1.6	5→3	1.62	6→4	2.245
1.7	5→2	1.46	6→3	2.04
1.8	5→2	1.28	6→3	1.84

squares denote the transition temperatures at which the number of penetrating/expulsing vortices changes. It is clear that the critical temperature is very sensitive to the value of $\xi(0)/b$ and the superconducting/normal transition moves to temperatures higher than T_{c0} comparing with Fig. 3. Moreover, the stability regions of different states overlap strongly. For the high temperature we only find the transitions with

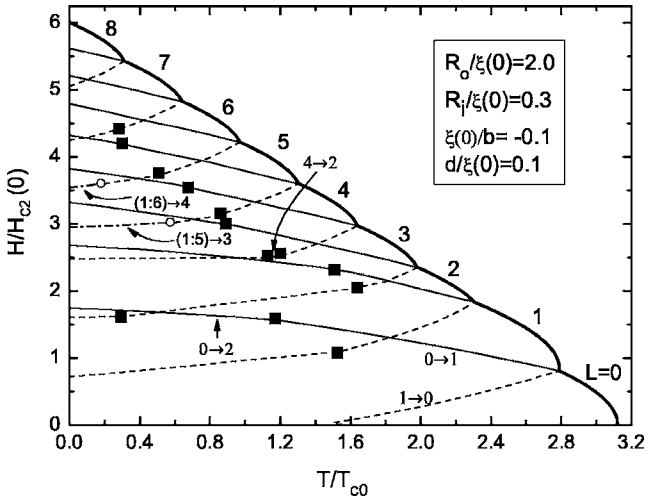

FIG. 8. The same as Fig. 3 but for $\xi(0)/b=-0.1$. The solid squares denote the transition temperatures at which the number of penetrating/expulsing vortices changes.

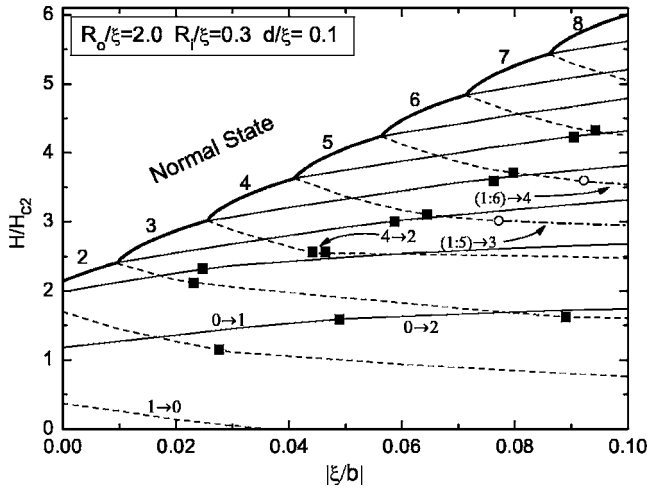

FIG. 9. The H-$|\xi/b|$ phase diagram for a ring with $R_o=2.0\xi$ and $R_i=0.3\xi$. The thick solid curves correspond to the nucleation fields $H_{\rm nuc}$. The thin solid and dashed curves denote the penetration fields H_p and the expulsion fields H_e, respectively. The solid squares denote the critical values of $|\xi/b|$ at which the number of penetrating/expulsing vortices changes.

$\Delta L=1$ and the transitions between the multivortex and giant vortex states also disappear. In addition, for the $4\rightarrow2$ transition we get that the temperature range is very small.

Now we investigate the influence of the surface enhancement on phase transition. Figure 9 gives the H-$|\xi/b|$ phase diagram for a ring with $R_i=0.3\xi$. The thick solid curves correspond to the nucleation fields $H_{\rm nuc}$, where $H_{\rm nuc}$ is the critical field for the transition between the superconducting state and the normal state. The thin solid and dashed curves denote the penetration fields H_p and the expulsion fields H_e, respectively. The solid squares denote the critical values of $|\xi/b|$ at which the number of penetrating/expulsing vortices changes. For the small values of $|\xi/b|$ or large vorticity L, only the transitions between the L and $L\pm1$ states can take place with increasing or decreasing field. Increasing the values of $|\xi/b|$, we find that the transitions with $\Delta L=2$ or 3 can occur, i.e., two or three vortices can simultaneously enter or leave the system with increasing or decreasing field, and the transitions between the multivortex and giant vortex states can be found.

Further increasing the surface enhancement of superconductivity, the multivortex states can exist in the ground state.[14] For a ring with $R_i=0.1\xi$ and $\xi/b=-0.2$, we find that there is a reentrant phase transition with the same vorticity for the (0:3) stable multivortex state, as predicted for the disks in Ref. 12, i.e., the giant vortex state transits to a multivortex state and then back to the same giant vortex state. Figure 10 shows the contour plots of the Cooper-pair density and phase of the order parameter for the (0:3) multivortex state at different magnetic fields. For the ring with $R_i=0.3\xi$ and $\xi/b=-0.2$, the stable $(1:L_2)$ states can be found as the ground state.[14] We find that the phase transitions between the stable multivortex states can occur for the small rings that we stuided. Figure 11(a) gives the free energy of the stable (1:5), (1:6), (1:7), and (1:8) states as well as the saddle-point states (1:5:8), which means the (1:8) state transits to the (1:5) state,

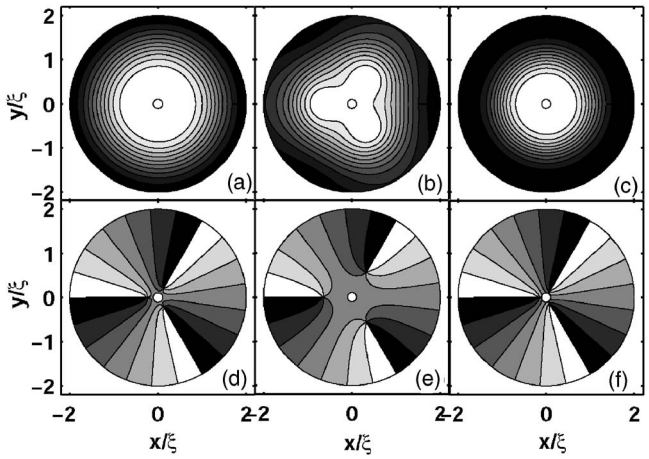

FIG. 10. The contour plot of the Cooper-pair density and phase of the order parameter for the (0:3) multivortex state at $H/H_{c2}=2.308$ (a), 2.82 (b), and 3.331 (c) for a superconducting ring with $R_o=2.0\xi$ and $R_i=0.1\xi$ and $\xi/b=-0.2$.

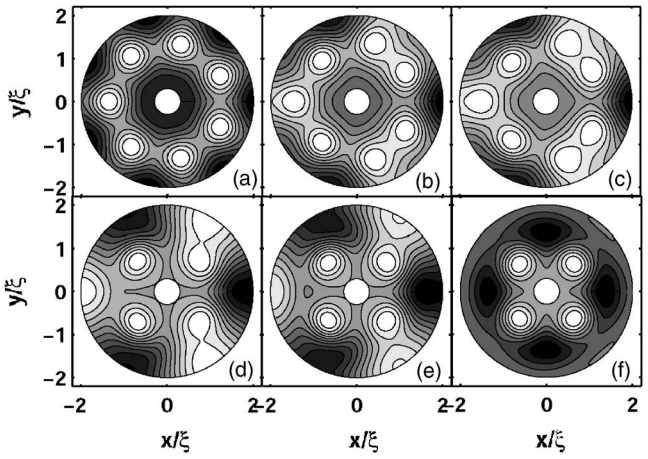

FIG. 12. Contour plot of the Cooper-pair density for the (1:5:8) state for the ring in Fig. 11 at $H/H_{c2}=4.227$ (a), 4.482 (b), 4.737 (c), 5.247 (d), 5.374 (e), and 5.504 (f).

and Fig. 11(b) shows the energy barriers U corresponding to the transitions $(1:8)\rightarrow(1:5)$ (solid curves) and the other possible transitions (dashed and dash-dotted curves). Due to the fact that the (1:5:8) state has the lowest energy barrier and the highest expulsion field, the transition $(1:8)\rightarrow(1:5)$ is most likely to occur. Figure 12 shows the contour plots of the Cooper-pair density for the (1:5:8) saddle-point state at different magnetic fields. For the (1:8) and (1:5) state, one vortex accommodates in the hole, while seven and four vortices are near the outer boundary, respectively. We can clearly see that three vortices move to the outer region of the ring with increasing field. Increasing the inner radius of the ring with $\xi/b=-0.2$, the $(2:L_2)$ states can also be found as the ground state.[14] Figure 13 gives the free energy (a) of the stable (2:7), (2:8), (2:9), and (2:10) states and the saddle-point state (2:7:10) as well as the energy barriers (b) corresponding to the transition $(2:10)\rightarrow(2:7)$ (solid curves) and the other possible transitions (dashed and dash-dotted curves) for a ring with $R_i=0.5\xi$ and $\xi/b=-0.2$. Notice that the transition between the (2:9) and (2:10) states cannot be found and only exist in the $(2:10)\rightarrow 9$ transition. For the (2:7:10) state, it has the lowest energy barrier and the highest expulsion field. Figure 14 gives the contour plots of the Cooper-pair density for the (2:7:10) state at different mag-

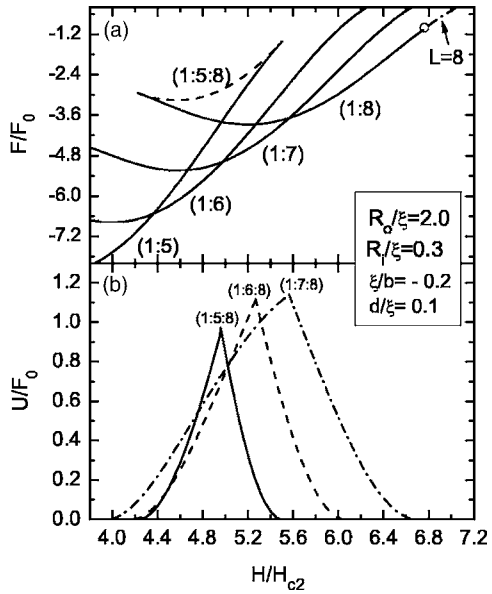

FIG. 11. (a) The free energy of the stable (1:5), (1:6), (1:7), and (1:8) states, and the saddle-point state (1:5:8) between (1:5) and (1:8) states for a superconducting ring with $R_o=2.0\xi$ and $R_i=0.3\xi$ and $\xi/b=-0.2$. (b) The energy barriers U correspond to the transition $(1:8)\rightarrow(1:5)$ (solid curves) and the other possible transitions (dashed and dash-dotted curves).

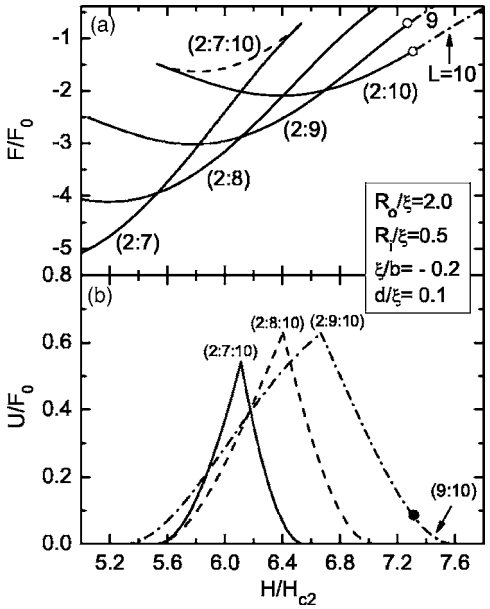

FIG. 13. (a) The free energy of the stable (2:7), (2:8), (2:9), and (2:10) states, and the saddle-point state (2:7:10) between (2:7) and (2:10) states for a superconducting ring with $R_o=2.0\xi$ and $R_i=0.5\xi$ and $\xi/b=-0.2$. (b) The energy barriers U correspond to the transition $(2:10)\rightarrow(2:7)$ (solid curves) and the other possible transitions (dashed and dash-dotted curves).

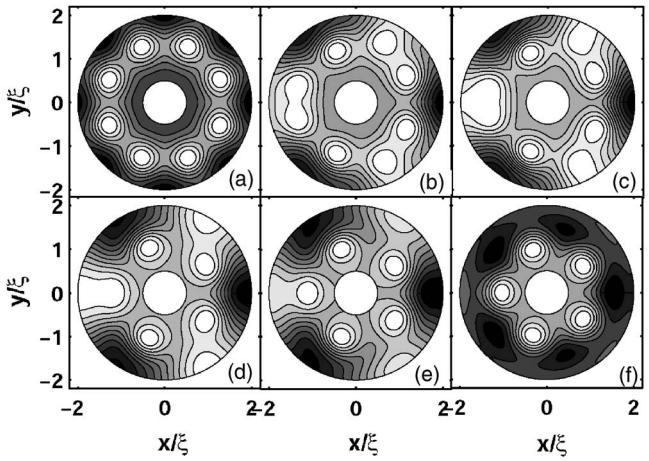

FIG. 14. Contour plot of the Cooper-pair density for the (2:7:10) state for the ring in Fig. 13 at H/H_{c2}=5.53 (a), 5.73 (b), 5.93 (c), 6.33 (d), 6.45 (e), and 6.545 (f).

netic fields and three vortices being expelled from the system with increasing field.

IV. LARGE RINGS

We consider now the relatively large superconducting rings surrounded by a medium that enhances superconductivity at the sample surface with fixed outer radius $R_o=4.0\xi$ and thickness $d=0.1\xi$. As an example, Fig. 15 gives the free energies of the different vortex states for a superconducting ring with $\xi/b=-0.1$ and $R_i=0.5\xi$ for $L\leqslant 14$. Notice that the (1:4:12), (1:5:13), and (1:5:14) states can be found as the metastable state and the ground state. We can get this clearly from the inset in Fig. 15. With increasing field, the ground state changes as follows:

$$0 \rightarrow 1 \rightarrow 2 \rightarrow (0:3) \rightarrow (0:4) \rightarrow (1:5) \rightarrow (1:6) \rightarrow (1:7) \rightarrow (1:8) \rightarrow (1:9) \rightarrow (1:10) \rightarrow (1:11) \rightarrow (1:4:12) \rightarrow (1:12) \rightarrow (1:5:13) \rightarrow (1:13) \rightarrow (1:5:14) \rightarrow \cdots .$$

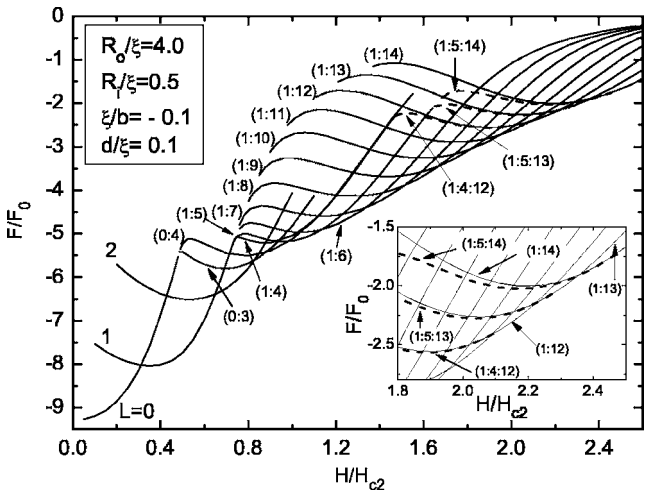

FIG. 15. The free energy for different vortex states in a superconducting ring with $R_o=4.0\xi$ and $\xi/b=-0.1$ and $R_i=0.5\xi$ for $L\leqslant 14$. The inset shows the (1:4:12), (1:5:13), and (1:5:14) states in more detail.

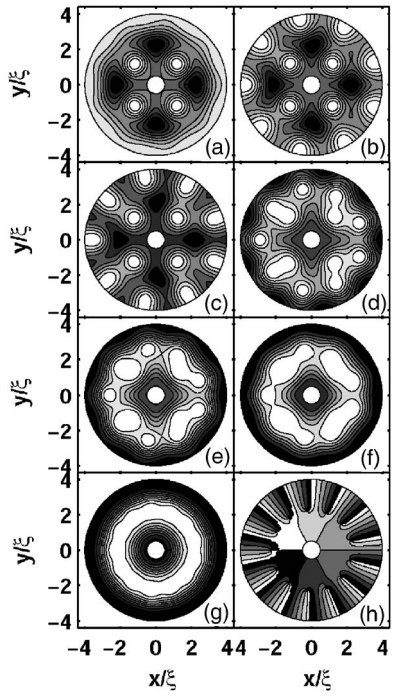

FIG. 16. Contour plot of the Cooper-pair density and phase of the order parameter (h) for a ring with $R_o=4.0\xi$ and $R_i=0.5\xi$ and $\xi/b=-0.1$ corresponding to the (1:5:14) state (a), (b), (c), (d), (e), (f), and (g) at H/H_{c2}=1.684, 1.696, 1.72, 2, 2.3, 2.4, and 2.492, respectively.

Figure 16 gives the contour plots of the Cooper-pair density at different magnetic fields corresponding to the (1:5:14) stable state. With increasing field, nine vortices enter the system and merge together with four other vortices forming one shell, meanwhile one vortex sits in the hole [see Figs. 16(a)–16(g)]. Figure 16(h) shows the contour plot of the phase of the order parameter corresponding to Fig. 16(g), indicating clearly that there exists one vortex in the hole and the other 13 vortices are positioned on a single shell around the center. Moreover, notice that two stable vortex shells can exist in the rings that we studied. (Note: two stable vortex shells had not been found for the disk of radius $R=4\xi$.[6]) In Fig. 17, the contour plots of the Cooper-pair density for the (0:3:12) state at $H/H_{c2}=1.6$ (a), the (1:5:14) state at $H/H_{c2}=1.74$ (b), and the (2:7:16) state at $H/H_{c2}=2.02$ (c) in the

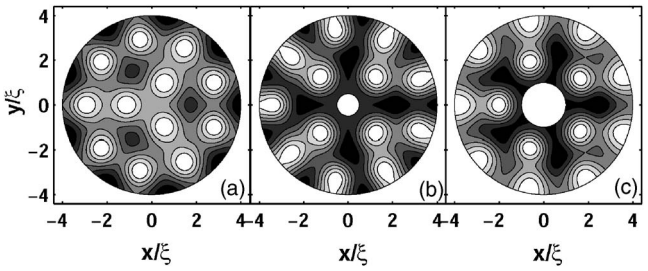

FIG. 17. Contour plot of the Cooper-pair density for the rings with $R_o=4.0\xi$ and $\xi/b=-0.1$ and $R_i=0.0\xi$ (a), $R_i=0.5\xi$ (b), and $R_i=1.0\xi$ (c) corresponding to the (0:3:12) state at $H/H_{c2}=1.6$, the (1:5:14) state at $H/H_{c2}=1.74$, and the (2:7:16) state at $H/H_{c2}=2.02$, respectively.

rings with $\xi/b=-0.1$ and $R_i=0.0\xi$, $R_i=0.5\xi$, and $R_i=1.0\xi$ are given, respectively. We can see that an inner shell and an outer shell exist in these rings, meanwhile one vortex sits in the hole for the (1:5:14) state and two vortices for the (2:7:16) state. Therefore, for the (L_1,L_2,L_3) state in a large ring there exist an inner shell with (L_2-L_1) vortices and an outer shell with (L_3-L_2) vortices, and L_1 vortex (vortices) is (are) located on the hole.

V. CONCLUSIONS

In summary, we have investigated the phase transitions for the thin mesoscopic superconducting rings surrounded by a medium that enhanced its superconductivity near the boundary through the phenomenological Ginzburg-Landau theory. The ring has more than one boundary in comparison with a disk sample and its vortex properties can be strongly influenced by the surface enhancement of superconductivity, so more complex and interesting features were found. For a small ring, we studied the transitions between different giant vortex states as well as between the giant vortex and multivortex states with increasing or decreasing the magnetic field, and the transitions with $\Delta L>1$, which can only exist in large size when the parameter $1/b$ tends to zero, were found with increasing the surface enhancement. We obtained the H-$|\xi/b|$, H-R_i, and H-T phase diagrams and studied the influences of the surface enhancement and the inner radius as well as the temperature on phase transition, respectively. Further increasing the surface enhancement of superconductivity, the reentrant transition ("*giant vortex→multivortex →giant vortex*") with the same vorticity was found for a small ring inner radius. Moreover, the transitions between the stable multivortex states with $\Delta L>1$ were revealed for different inner radii in the small rings. For a relatively large ring, we investigated the vortex configurations and found that the vortex state with two stable vortex shells can exist in the ground state due to the enhanced surface superconductivity.

ACKNOWLEDGMENTS

This work was supported by the National Natural Science Foundation of China (Grant No. 60371033) and by Shanghai Leading Academic Discipline Program, China.

*Electronic address: zgq_1981@graduate.shu.edu.cn
†Author to whom all correspondence should be addressed. Electronic address: shipingzhou@online.sh.cn

[1] V. V. Moshchalkov, L. Gielen, C. Strunk, R. Jonckheere, X. Qiu, C. Van Haesendonck, and Y. Bruynseraede, Nature (London) **373**, 319 (1995); A. K. Geim, I. V. Grigorieva, S. V. Dubonos, J. G. S. Lok, J. C. Maan, A. E. Filippov, and F. M. Peeters, *ibid.* **390**, 259 (1997); A. Kanda, B. J. Baelus, F. M. Peeters, K. Kadowaki, and Y. Ootuka, Phys. Rev. Lett. **93**, 257002 (2004).
[2] P. S. Deo, V. A. Schweigert, F. M. Peeters, and A. K. Geim, Phys. Rev. Lett. **79**, 4653 (1997); V. A. Schweigert and F. M. Peeters, Phys. Rev. B **57**, 13817 (1998); Phys. Rev. Lett. **83**, 2409 (1999); P. S. Deo, V. A. Schweigert, and F. M. Peeters, Phys. Rev. B **59**, 6039 (1999); B. J. Baelus, F. M. Peeters, and V. A. Schweigert, *ibid.* **61**, 9734 (2000); G. F. Zharkov, *ibid.* **63**, 224513 (2001); J. Bonča and V. V. Kabanov, *ibid.* **65**, 012509 (2002); B. J. Baelus and F. M. Peeters, *ibid.* **65**, 104515 (2002); Shi-Ping Zhou, Yao-Ming Shi, Bao-He Zhu, and Guo-Qiao Zha, *ibid.* **73**, 174503 (2006).
[3] V. A. Schweigert, F. M. Peeters, and P. S. Deo, Phys. Rev. Lett. **81**, 2783 (1998).
[4] V. A. Schweigert and F. M. Peeters, Physica C **332**, 266 (2000).
[5] J. J. Palacios, Phys. Rev. Lett. **84**, 1796 (2000); Physica C **332**, 263 (2000).
[6] J. J. Palacios, Physica B **256**, 610 (1998); Phys. Rev. B **58**, R5948 (1998).
[7] B. J. Baelus, F. M. Peeters, and V. A. Schweigert, Phys. Rev. B **63**, 144517 (2001).
[8] B. J. Baelus, L. R. E. Cabral, and F. M. Peeters, Phys. Rev. B **69**, 064506 (2004).
[9] P. G. de Gennes, *Superconductivity of Metals and Alloys* (Addison-Wesley, New York, 1994).
[10] P. G. de Gennes and J. Matricon, Rev. Mod. Phys. **36**, 45 (1964).
[11] W. V. Pogosov, Phys. Rev. B **65**, 224511 (2002).
[12] S. V. Yampolskii and F. M. Peeters, Phys. Rev. B **62**, 9663 (2000).
[13] B. J. Baelus, S. V. Yampolskii, F. M. Peeters, E. Montevecchi, and J. O. Indekeu, Phys. Rev. B **65**, 024510 (2002).
[14] Guo-Qiao Zha, Shi-Ping Zhou, and Bao-He Zhu, Phys. Rev. B **73**, 092512 (2006).
[15] Guo-Qiao Zha, Shi-Ping Zhou, Bao-He Zhu, and Yao-Ming Shi, Phys. Rev. B **73**, 104508 (2006).
[16] *Handbook of Mathematical Functions*, edited by M. Abramowitz and I. A. Stegun (Dover, New York, 1970), p. 504.
[17] M. V. Milošević, S. V. Yampolskii, and F. M. Peeters, Phys. Rev. B **66**, 024515 (2002).